A&A 493, 1155–1160 (2009)
DOI: 10.1051/0004-6361:200810294

Astronomy & Astrophysics

Collisional effects in the far red wing of Lyman-α

N. F. Allard[1,2] and J. F. Kielkopf[3]

[1] Observatoire de Paris, GEPI, UMR 8111, CNRS, 61 avenue de l'Observatoire, 75014 Paris, France
e-mail: nicole.allard@obspm.fr
[2] Institut d'Astrophysique de Paris, UMR 7095, CNRS, Université Pierre et Marie Curie, 98bis boulevard Arago, 75014 Paris, France
[3] Department of Physics and Astronomy, University of Louisville, Louisville, KY, 40292, USA

Received 30 May 2008 / Accepted 14 October 2008

ABSTRACT

Context. An accurate determination of the line broadening of the Lyman series of atomic hydrogen has been shown to be fundamental to interpretating UV and FUV spectra of DA white dwarfs. Quasi-molecular lines have been detected in the red wing of Lyman-α, Lyman-β, and Lyman-γ. They arise from radiative collisions of excited atomic hydrogen with unexcited neutral hydrogen atoms or protons.
Aims. The aim of this paper is twofold. First, we examine the range of validity of the one-perturber approximation widely used to calculate the line wing. Second, we study the relative contributions of the two main transitions contributing to the far wing of the Lyman-α line profile according to the effective temperature and perturber density.
Methods. In cool white dwarfs, the perturber density is so high that the one-perturber approximation breaks down and the collisional effects must be treated by using the autocorrelation formalism in order to take into account simultaneous collisions with more than one perturbing atom.
Results. We show that, at the low temperatures of cool white dwarfs, the contribution of the singlet $X^1\Sigma_g^+ \rightarrow B^1\Sigma_u^+$ transition cannot be neglected in the calculation of Lyman-α profile perturbed by neutral hydrogen. A comparison with experimental laboratory spectra shows that the effects of multiple H-perturbers appear in the far wing.
Conclusions. A reliable determination of the line profiles for the physical conditions of cool white dwarfs requires a unified theory that takes account of both the singlet and triplet transitions contributing to Lyman-α using accurate interaction potentials and radiative dipole transition moments. Multiple perturber effects must be considered and the autocorrelation formalism permits calculations for the densities of the atmospheres of cool white dwarfs.

Key words. stars: white dwarfs – line: profiles – radiation mechanisms: general – stars: atmospheres

1. Introduction

In Allard & Kielkopf (1991), we presented calculations of the dependence on temperature and density of the resonance broadening in the far wing of the Lyman-α line for atmospheres of DA white dwarfs. We highlighted the importance of the close collisions of many perturbers, which leads to the formation of a series of satellites in the far red wing of Lyman-α. We emphasized that these effects would provide a previously unrecognized source of opacity for the photosphere of a DA white dwarf when it cools to below 10 000 K. As a consequence, we concluded the far wing of Lyman-α becomes an important consideration when the age of the galactic disk is estimated from the luminosity function of very cool white dwarfs.

In Allard et al. (2004), we presented a study of the influence of temperature on the line wing and satellites of the Lyman-α absorption profiles, and compared synthesized absorption spectra with HST spectra of ZZ Ceti white dwarfs, typically at temperatures from 10 000 to 15 000 K. In this paper, we extend that work to the physical conditions of very cool white dwarfs with $T_{\rm eff}$ below 5000 K. We restrict our study to the collisional effects due to atomic hydrogen.

It is of considerable interest to determine line profiles in these extreme physical conditions. A small fraction of the DA white dwarfs are known to have effective temperatures $T_{\rm eff} \leq$ 4000 K. Such objects were discussed by Wolff et al. (2002) and Kowalski & Saumon (2006).

2. Theory

2.1. Correlation diagram

The correlation diagram in Fig. 1 allows us to identify the molecular transitions that contribute to Lyman-α. Solid and dotted lines are respectively used for singlet and triplet states. The version shown here corrects one presented in Allard et al. (1994) in which the labels of the a and h triplet states were interchanged. The correct correlation diagram shown here was used in Allard et al. (1998), and in our subsequent work, but the correction was not clearly explained in that paper.

In Allard et al. (1999), we developed a new theory taking into account the dependence on interatomic distance of the transition probability of allowed and asymptotically forbidden transitions. Our approach, which introduces the concept of a modulated dipole transition moment into the calculation of the line shape, allows us to take into account the two asymptotically forbidden transitions ($X^1\Sigma_g^+ \rightarrow B'^1\Sigma_u^+$ and $b^3\Sigma_u^+ \rightarrow h^3\Sigma_g^+$) of quasi-molecular hydrogen that dissociate into $(1s, 2s)$ atoms. Our results show that they constitute a minor contribution compared with the other transitions.

Collisions of neutral H atoms contribute strongly to the red wing of Lyman-α through transient singlet states of H_2. The $B^1\Sigma_u^+ \rightarrow X^1\Sigma_g^+$ and $C^1\Pi_u \rightarrow X^1\Sigma_g^+$ free-free transitions lead to quasi-molecular line satellites corresponding to the Lyman and Werner H_2 bands. These satellites were observed in experimental

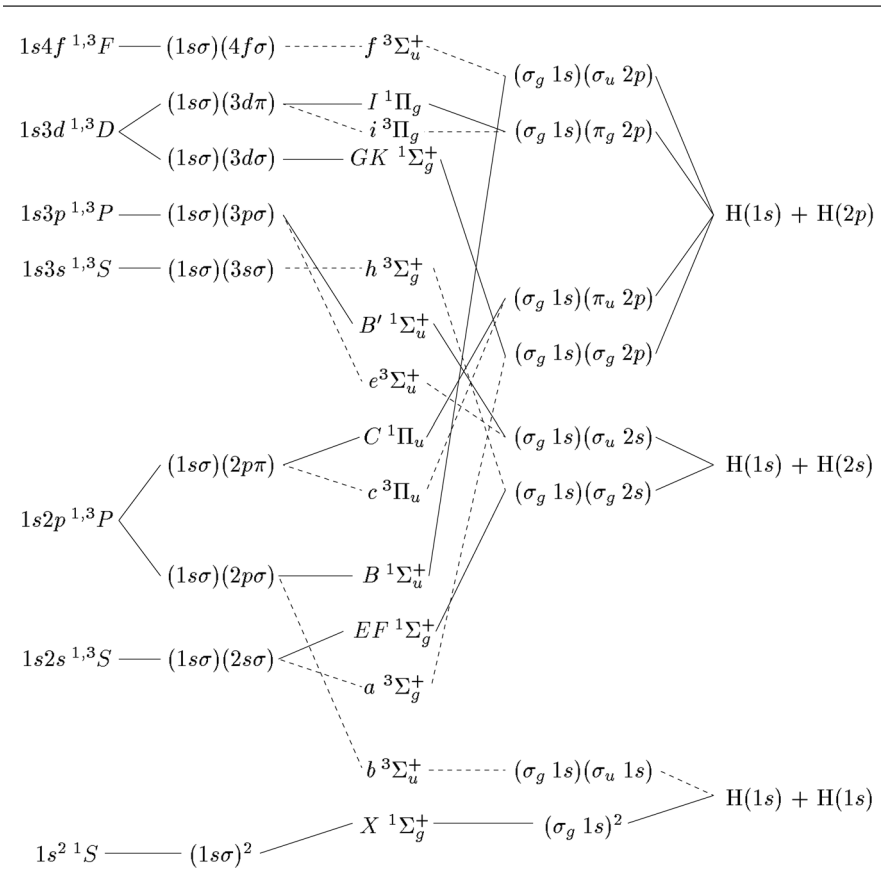

Fig. 1. Correlation diagram for H_2 states contributing to Lyman-α.

spectra of laser-produced plasma sources, which simulate white dwarf atmospheric conditions in the laboratory (Kielkopf & Allard 1995).

2.2. Molecular data

We use the molecular data of Spielfiedel (2003) and Spielfiedel et al. (2004). In Fig. 2, we have plotted the potential energies of the 2 transitions that contribute most to the far red wing of the Lyman-α: the triplet transition $b\ ^3\Sigma_u^+ \rightarrow a\ ^3\Sigma_g^+$ and the singlet $X^1\Sigma_g^+ \rightarrow B^1\Sigma_u^+$ transition.

In Fig. 3, we have plotted the potential difference related to the $b^3\Sigma_u^+ \rightarrow a^3\Sigma_g^+$ transition, together with the modulated dipole moment of this transition for different temperatures. The corresponding figure for the singlet $X^1\Sigma_g^+ \rightarrow B^1\Sigma_u^+$ transition is given in Fig. 2 of Allard et al. (2004). The radiative electric dipole transition moment of each component of the line depends on R, and changes during the collision. In Allard et al. (1999), we defined $\tilde{\mathrm{d}}_{ee'}(R(t))$ as a *modulated* dipole given by (Allard et al. 1999)

$$D(R) = \tilde{\mathrm{d}}_{ee'}[R(t)] = \mathrm{d}_{ee'}[R(t)]\mathrm{e}^{-\frac{V_e[R(t)]}{2kT}}, \quad (1)$$

where the potential energy for the initial state was

$$V_e(R) = E_e(R) - E_e^{\infty}. \quad (2)$$

The difference potential energies $\Delta V(R)$ for a transition ee' is

$$\Delta V(R) = V_{e'e}(R) = V_{e'}(R) - V_e(R). \quad (3)$$

This figure will help us to understand the effects, due to this transition, on the profile as the temperature varies as discussed below.

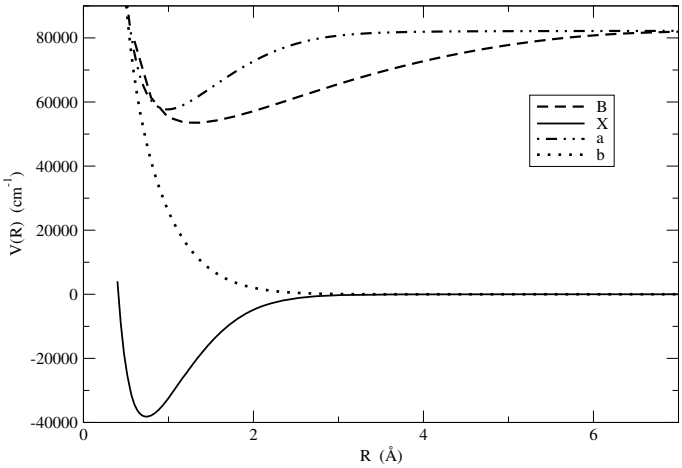

Fig. 2. Molecular potentials for $b \rightarrow a$ and $X \rightarrow B$ transitions. The energies are given relative to the asymptotic atomic state.

3. Variation in line profiles at 10 000 K with density of neutral hydrogen

Many problems in collision-induced, radiative transitions have been solved by using the one-perturber approximation. At very low densities, the binary model for an optically active atom in collision with one perturber is valid for the entire profile, apart from the central part of the line.

Semi-classical and quantum calculations of the wing of Lyman-α were first developed by Sando et al. (1969) and

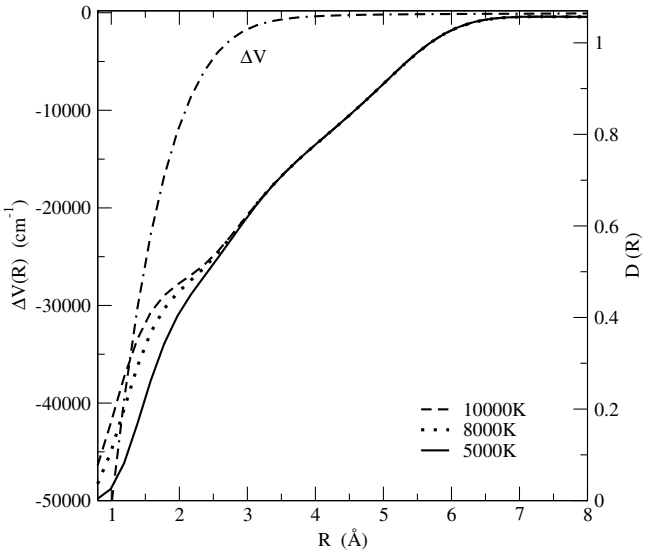

Fig. 3. Variation with temperature in the modulated dipole and the difference potential of the $b \rightarrow a$ transition.

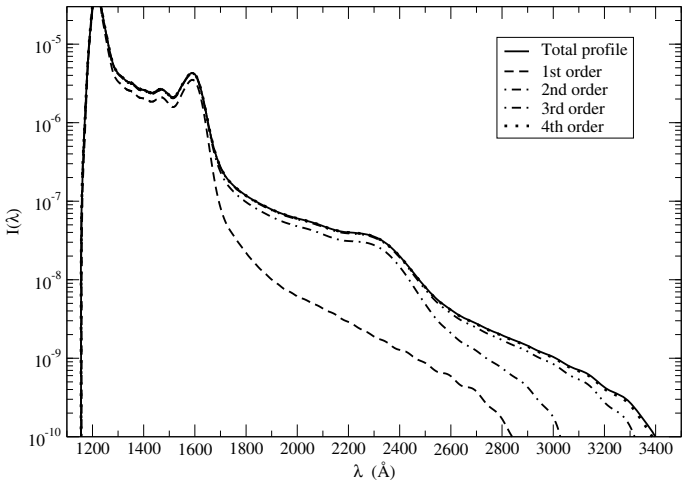

Fig. 4. Contribution of the different orders of the expansion to the profile for $T = 10\,000$ K and $n_{\rm H} = 10^{21}$ atoms cm^{-3}.

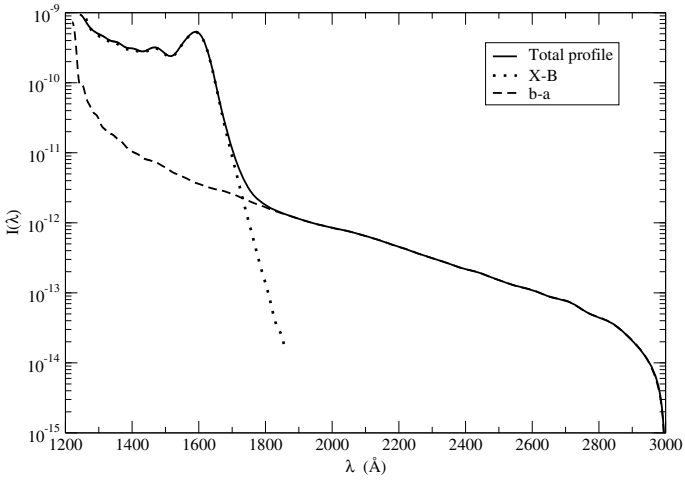

Fig. 5. Contribution of the $X \rightarrow B$ and $b \rightarrow a$ transitions to the red wing for $T = 10\,000$ K and $n_{\rm H} = 10^{17}$ atoms cm^{-3}.

Sando & Wormhoudt (1973). The semi-classical methods used by Sando & Wormhoudt (1973) were generalized for applying to entire profiles in the unified Franck-Condon theory of Szudy & Baylis (1975). This method has been used widely for the analysis of line-broadening experiments (Allard & Kielkopf 1982). Its simplicity derives from a neglect, in the line wing, of multiple close collisions. The profiles computed with this approach provide a unified expression from the line core to the wing. However, in the satellite region of the line wing the results are only valid when densities are so low that the probability of close collision of more than two atoms is negligibly small in comparison to the contributions from binary collisions. In real systems, multiple perturber collisions cannot be neglected beyond the satellite except at very low density.

An exact methodology for the quantum calculation at high densities, as encountered in stellar atmospheres or laboratory plasmas, is unknown. However, the results of their quantum calculation are also reproduced by a semi-classical approach, and are a successful test of the semi-classical methods. Fortunately, the semi-classical methods can also be extended by unified theories of line broadening to permit an inclusion of the effects of multiple collisions (Allard & Kielkopf 1982). The density expansion (Royer 1971, 1978) enables the accurate numerical evaluation of the far wing possible for many conditions of astrophysical interest. Figure 4 shows the total profile that takes into account the 4 allowed transitions, the $X^1\Sigma_g^+ \rightarrow B^1\Sigma_u^+$ and $X^1\Sigma_g^+ \rightarrow C^1\Pi_u$ singlet transitions, and the $b\,^3\Sigma_u^+ \rightarrow a\,^3\Sigma_g^+$ and $b^3\Sigma_u^+ \rightarrow i^3\Pi_g^+$ triplet transitions. The red wing is dominated by the contribution of multiple-perturber collisions, and the expansion of the autocorrelation function in density must be completed to the fourth order to be comparable with the result obtained from a unified calculation.

In the following, we restrict our study to the singlet $X \rightarrow B$ and triplet $b \rightarrow a$ transitions, the two transitions that contribute most to the red wing of the Lyman-α line. All calculations are completed using the density expansion to the seventh order.

The total profiles shown in the figures are the Fourier transforms of the correlation function given by Eq. (121) of Allard et al. (1999), in which the contributions from different components of the transition enter with their statistical weights. The figures also show the individual components for comparison, weighted as if they were the only contribution to the profile. The profiles presented here are applicable to wavelengths between the Lyman-α line and the far infrared.

3.1. Low and intermediate densities

Figure 5 shows the prominent satellite that arises from the $X^1\Sigma_g^+$–$B\,^1\Sigma_u^+$ free-free transition of a neutral hydrogen atom in the presence of other ground state atoms. The two-body H(1s)-H(2p) satellite is at approximately 1600 Å. It arises from the extremum of –20 200 cm^{-1} in the $X \rightarrow B$ difference potential, when the two atoms are separated by about 2 Å (see Fig. 2 of Allard et al. 2004). The contribution of the $X \rightarrow B$ transition is identical to the first order of the expansion shown in Fig. 5. At such a low density ($n_{\rm H} = 10^{17}$ atoms cm^{-3}), the one-perturber approximation is valid, and the total profile above 1800 Å is due to the triplet $b \rightarrow a$ transition.

When the H density is increased to $n_{\rm H} = 10^{20}$ atoms cm^{-3}, Fig. 6 shows that the far wing of the individual profile from the $X \rightarrow B$ transition above 1800 Å is due to multiple-perturber collisions. In a simple additive approximation, a three-body satellite to Lyman-α should result from an H(2p) atom radiating while it

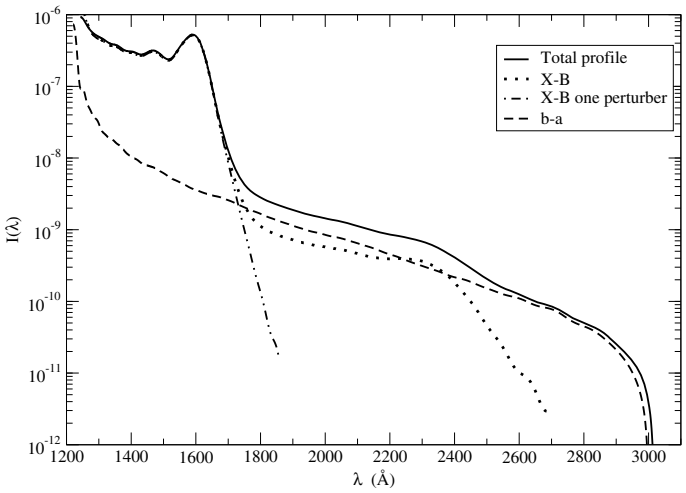

Fig. 6. Contribution of the $X \rightarrow B$ and $b \rightarrow a$ transitions to the red wing for $T = 10\,000$ K and $n_{\rm H} = 10^{20}$ atoms cm^{-3}.

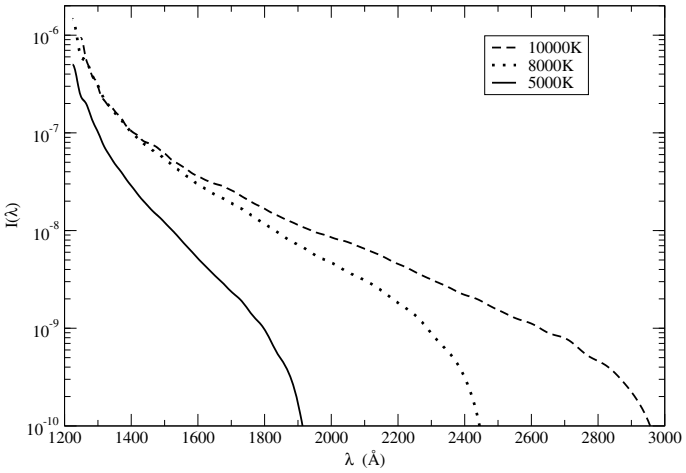

Fig. 7. Variation of the extension of the individual profile due to the $b \rightarrow a$ transition in the red wing for $T = 10\,000$ K, $T = 8000$ K, $T = 5000$ K for $n_{\rm H} = 10^{21}$ atoms cm^{-3}.

is close to two H(1s) atoms. A difference potential minimum of approximately $2 \times (-20\,200) = -40\,400$ cm^{-1} is expected in this case. The effect observed in laboratory spectra at 2500 Å discussed below is –45 300 cm^{-1} from the Lyman-α line center. At $n_{\rm H} = 10^{20}$ atoms cm^{-3} the total profile above 1800 Å is still primarily due to the $b \rightarrow a$ transition, but the $X \rightarrow B$ second satellite begins to contribute to the amplitude of the far wing.

3.2. High density

When the density is as high as $n_{\rm H} = 10^{21}$ atoms cm^{-3} (Fig. 4), the one-perturber binary approximation is no longer valid. The amplitude of the first satellite is linear with density until 10^{21}, but for 3×10^{22}, the amplitude of the first satellite begins to decrease with increasing density. When this density is reached, the probability of a collision with two perturbers is higher than the probability of a collision with only one perturber (see e.g. Allard 1978; Royer 1978). Theoretically, as shown by Royer (1971), the probability of m perturbers in a volume V is shown in Fig. 27 of Allard & Kielkopf (1982). These variations in amplitude of the first and second satellites are well explained using a square well potential, as is shown in the analysis of Allard (1978) (Fig. 5), and also reported in Allard & Kielkopf (1982) (Figs. 18 and 19). This dependence on the average number of perturbers in the collision volume is expected on the basis of the Poisson distribution, which indicates the probability of finding a select number of uncorrelated perturbers in this collision volume. It was first identified in experimental alkali spectra by Exton & Snow (1978) and by Kielkopf & Allard (1979).

4. Variation with temperature

The appearance of an extended wing shown in Fig. 7 is sensitive to temperature because of the variation in modulated transition dipole moment with temperature. Figure 3 illustrates that there is no contribution from triplets above 1900 Å (–30 000 cm^{-1}) for $T = 5000$ K because the modulated transition dipole moment is too weak.

Figures 8 and 9 show how the line profiles vary as the temperature decreases from $T = 8000$ K to 5000 K. The $X \rightarrow B$ and $b \rightarrow a$ quasi-molecular transitions both contribute and must be included. In Fig. 8, we have compared the total profile, for which multiple perturber effects are taken into account, with the

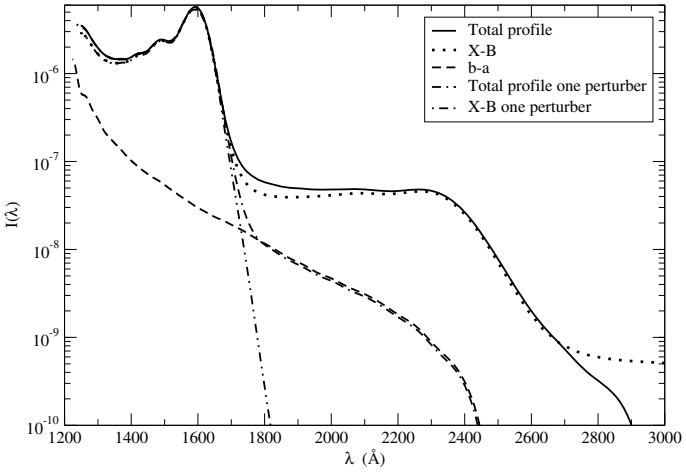

Fig. 8. Contribution of the $X \rightarrow B$ and $b \rightarrow a$ transitions to the red wing for $T = 8000$ K and $n_{\rm H} = 10^{21}$ atoms cm^{-3}.

total profile for when the expansion is stopped at first order, which is equivalent to the one perturber approximation. Due to the weighting, the singlet $X \rightarrow B$ provides only 1/3 of the total line far wing strength. Nevertheless, the contributions of singlet collisions with multiple perturbers dominate the 1800–3000 Å region. Consequently, the ultraviolet triplet $b \rightarrow a$ transition does not, in itself, account for the far red wing of the Lyman-α profile broadened by collisions with atomic hydrogen. In their analysis of the missing opacity in cool, dense, white dwarf stars, Kowalski & Saumon (2006) did not include this effect.

5. Laboratory spectra

Satellites in the far wings of Lyman-α are seen in the emission spectra of plasmas produced when a pulsed laser excites an H_2 gas target (Kielkopf & Allard 1998). This earlier work on Lyman$-\alpha$ was based on experiments for conditions under which only binary collisions were important in the spectral regions up to 1600 Å that were analyzed. We have developed techniques to use initial pressures of above 100 atmospheres, yielding laser-produced plasmas with atomic densities over 10^{21} atoms cm^{-3} at the temperature of the atmosphere of a white dwarf. A preliminary report presented by Kielkopf & Allard (2000) described

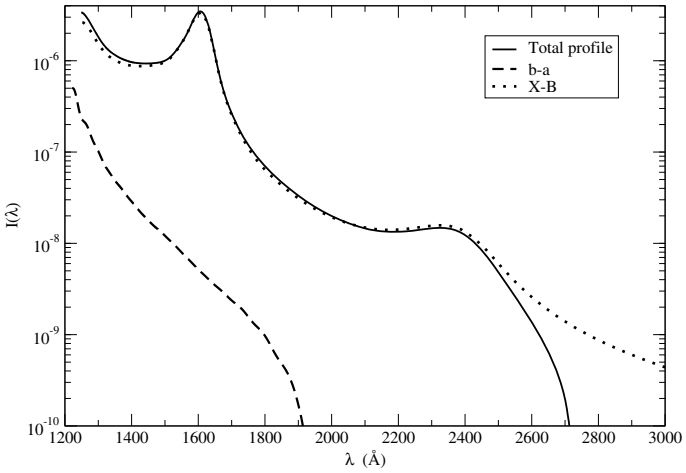

Fig. 9. Contribution of the $X \rightarrow B$ and $b \rightarrow a$ transitions to the red wing for $T = 5000$ K and $n_{\rm H} = 10^{21}$ atoms cm^{-3}.

measurements of high density sources that extended from the Lyman-α wing beyond the 1600 Å satellite, where the effects of more than one perturber acting simultaneously on the radiating atom are expected to appear.

5.1. Laser-produced plasmas: white dwarf atmospheres in the laboratory

A dense, hydrogen plasma produced by an energetic pulsed laser emits a continuous spectrum in the infrared, visible, ultraviolet, and vacuum ultraviolet spectral regions. The spectrum is time-dependent, arising in a nominally cylindrical shock propagating outward from the focus of the laser under predictable conditions (Kielkopf 1995, 2000).

For the data shown here, a pulsed Nd:YAG laser (1064 nm, 10 Hz, 300 mJ/pulse) was focused into a static cell filled with 99.999% pure H_2. The arrangement was similar to that described by Kielkopf & Allard (1998), except that the cell and its windows were designed to operate at elevated pressures. For spectra below 1850 Å, a 2 mm thick MgF_2 window separated the cell from the spectrograph, and because of window fragility the pressures were limited to 7 atmospheres. Above 1850 Å, a 3 mm thick fluorescence-free fused silica window permitted operation up to 125 atmospheres. Spectra shown here were recorded with a 0.2 m aberration-corrected holographic concave grating vacuum monochromator with a spectral resolution of 4 Å. They represent a portion of a comprehensive data set spanning from 1200 Å in the vacuum ultraviolet to 2.5 μm in the infrared. Below 1800 Å, a solar blind detector was used to minimize sensitivity to scattered light, but, at longer wavelengths, a sodium salicylate converter and UV-sensitive photomultiplier provided a nominally flat spectral response up to Balmer-β. Multichannel photon-counting in 5 ns wide bins recorded the development of the emission in a single spectral channel for 5 μs after each laser pulse, and accumulated time-tagged counts were averaged over 400 pulses. The spectral channel was sequentially stepped, and the acquisition was repeated. Slices in a fixed-width time-window across the spectrum provided snapshots of the development of the plasma's emission from its fully ionized initial state, a few nanoseconds after plasma production, to a cool, dense atomic gas 5 ms later.

In addition to the Lyman-α line broadened by neutral atomic collisions discussed here, there were contributions from collisions of the radiating atom with protons, from free-free and free-bound transitions of electrons in the field of protons, from the ionic molecules H^- and H_2^+, and from the radiative dissociation of neutral H_2.

The broadening of Lyman-α in proton collisions has been discussed elsewhere (Kielkopf & Allard 1998). It is important at wavelengths below 1450 Å in highly ionized hydrogen plasmas, but there is no significant contribution from these ionic collisions in the spectral region above 1450 Å during the cooling temporal domain discussed here. However, we are able to observe that the temperatures of the laser plasmas measured in this experiment are sufficiently high that there are no bound H_2 molecules either. It is a weakly ionized, dense, atomic plasma. From 1450 Å to 3000 Å, the observable continuum is due entirely to radiative, neutral, atomic collisions associated with the long wavelength "red" wing of Lyman-α.

Above 3000 Å, approaching the Balmer series limit at 3646 Å, the other contributions noted above become increasingly important. They are well known and analytical formulations are given by Roberts & Voigt (1971) that may be used to extract a plasma temperature by fitting the continuum in this region. Since the shock-driven, plasma model predicts a temperature T and density profile in the plasma, there is a model density $n_{\rm H}$ of atomic H corresponding to each spectroscopic temperature. This density is qualitatively similar to that found in the plasma region where the $n = 2$ state, the upper state of Lyman-α, has its maximum population. A spectroscopic temperature and density determined in this way is completely independent of theoretical unified theory modeling of the Lyman-α line-broadening by neutral, atomic hydrogen.

5.2. Results

Experimental data for initial H_2 pressures between 7 and 120 atmospheres were recorded from 1200 Å in the vacuum ultraviolet to 2.5 μm in the infrared. Portions of two runs, one for the range 1450–1850 Å and the other for 1850–3000 Å, are shown in Fig. 10. For the shorter wavelength data, the spectroscopic diagnostics and plasma model establish an atomic hydrogen density of $n_{\rm H} = 3.7 \times 10^{20}$ atoms cm^{-3} and a temperature of $T = 4100$ K. For the longer wavelength data, acquired for a higher initial density, the parameters are $n_{\rm H} = 5.9 \times 10^{21}$ atoms cm^{-3} and a temperature of $T = 5600$ K. The two data sets are scaled so that they match at the wavelength at which they join. This simple representation allows us to present a qualitative picture of the far wing of the Lyman-α, quasi-molecular continuum emitted by the plasma.

The prominent 1600 Å satellite is due to free-free transitions of atomic H in the 2p state radiating during a collision with a ground state 1s H atom. The other weak feature, at 2500 Å, is attributed to "two-perturber" collisions in which the atom radiates while *two* 1s atoms are nearby. Previously, such two-perturber (and higher order) effects have been observed in several cases, including by a comprehensive study of Tl broadened by noble gases and compared to unified theory calculations with a priori potentials (Kielkopf 1983). In atomic H, such effects contribute to the opacity far into the red wing of Lyman-α, and are thus important to include in atmosphere models and synthetic spectra of cool white dwarfs. The observed spectrum in Fig. 10 is compared to a theoretical spectrum computed for a density intermediate between that of the two data sets. The observed profiles are consistent with the theoretical model although the satellite at

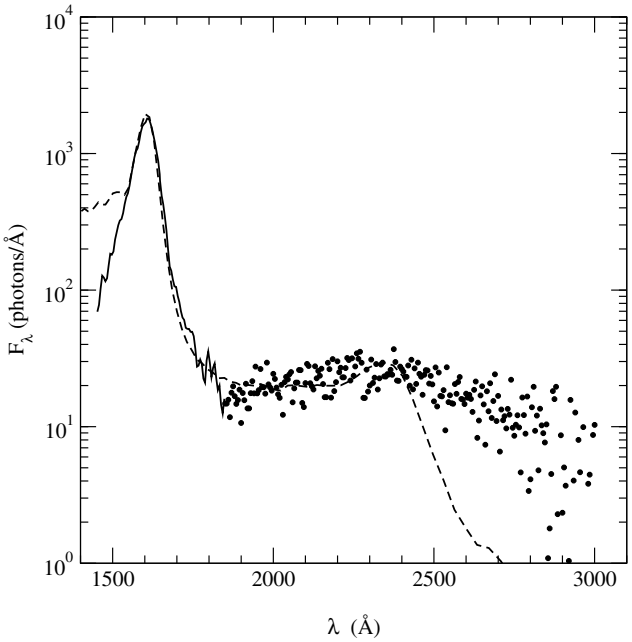

Fig. 10. Comparison of experimental profiles to the theoretical one calculated for $T = 4100$ K and $n_H = 2.5 \times 10^{21}$ atoms cm^{-3}. Measurements below 1850 Å (—) were completed for a plasma at 3.7×10^{20} atoms cm^{-3} at $T = 4100$ K. Measurements above 1850 Å ($\cdots$) were completed for a 5.9×10^{21} atoms cm^{-3} plasma at $T = 5600$ K. The two experimental data sets were scaled to match at the wavelength at which they join. The observed continuum enhancement at 2500 Å is consistent with the predicted multiple-perturber effect on Lyman-α exhibited by the theoretical profile.

2500 Å appears to have a different shape than predicted by the additive approximation for the atomic interaction.

6. Synthetic spectra of cool white dwarfs

Previous Lyman-α line-profile calculations were completed at low temperatures and included in atmosphere models by Wolff et al. (2002), and by Kowalski & Saumon (2006).

Both papers compared synthetic spectra with observed spectra of BPM4729. Unfortunately, neither paper showed the actual line profiles that were used, and it is therefore impossible to compare our work directly with theirs. However, we note that in Fig. 3 of Wolff et al. (2002), the change in slope of the synthetic spectrum is certainly due to the second satellite. Their predicted profile in a pure hydrogen atmosphere does not agree with observations. Since the transitions and the corresponding potentials used were not specified in the paper, we cannot draw a conclusion about the reason for the discrepancy. Kowalski & Saumon (2006) were successful in reproducing the spectrum of BPM4729 from the ultraviolet to near IR. They used a line profile calculated in the quasi-static approximation for only the $b \rightarrow a$ transition in H-H collisions, and they also included collisions with H_2, but the transitions and symmetries for the corresponding H_3 potentials, which have been taken into account in this work, are not given in the paper. We have seen in our work reported here that the $b \rightarrow a$ transition alone is inadequate to account for the spectrum above 1600 Å at elevated atomic hydrogen densities.

7. Conclusion

Many-body free-free collisions in dense atomic H have been shown to perturb the 2p atomic state to the extent that photons are emitted in the ultraviolet, rather than in the vacuum ultraviolet. Extrema in the difference potential-energy surfaces give rise to satellites in the far wing of Lyman-α. The intensity of these satellites depends on the probability of the collision that produces them, and on the radiative dipole moment of the transient multi-atom system. The probability increases with atomic density, and is enhanced by the collision dynamics and the Boltzmann factor of the excited state. The radiative dipole moment changes significantly in close collisions from its asymptotic value for the unperturbed atom.

One such satellite, corresponding to a transition to H(2p)-H(1s)-H(1s), appears in emission from a laser-produced plasma with an atomic H density on the order of 10^{20} atoms cm^{-3}. The observed spectral line profile is consistent with a unified line-shape theory that includes contributions from the triplet states. Transitions from the B to the X state for unbound atoms in collision are primarily responsible for the emission between 1500 Å and 3000 Å. Cool, white dwarfs require a special treatment because of the high perturber density involved. Homeier et al. (2007) investigated effects on the Na doublet of the high perturber densities occurring in metal-rich white dwarfs with a helium-dominated atmosphere. The density of neutral, atomic helium as a perturber of hydrogen Lyman-α in two cool white dwarfs exhibiting strong Na absorption could reach 10^{22} atoms cm^{-3}. Homeier et al. (2007) demonstrated that successful modeling of spectra at high perturber density requires a unified theory that takes into account multiple perturber effects.

References

Allard, N. F. 1978, J. Phys. B: Atom. Molec. Phys., 11, 1383
Allard, N. F., & Kielkopf, J. F. 1982, Rev. Mod. Phys., 54, 1103
Allard, N. F., & Kielkopf, J. F. 1991, A&A, 242, 133
Allard, N. F., Koester, D., Feautrier, N., & Spielfiedel, A. 1994, A&AS, 108, 417
Allard, N. F., Drira, I., Gerbaldi, M., Kielkopf, J. F., & Spielfiedel, A. 1998, A&A, 335, 1124
Allard, N. F., Royer, A., Kielkopf, J. F., & Feautrier, N. 1999, Phys. Rev. A, 60, 1021
Allard, N. F., Kielkopf, J. F., & Loeillet, B. 2004, A&A 424, 347
Exton, R., & Snow, 1978, JQRST, 20, 1
Homeier, D., Allard, N. F., Johnas, C. M. S., Hauschildt, P. H., & Allard, F. 2007, ASP Conf. Ser. 372, 15th European Workshop on White Dwarfs, 277
Kielkopf, J. F. 1983, J. Phys. B: At. Mol. Opt. Phys., 16, 3149
Kielkopf, J. F. 1995, Phys. Rev. E, 52, 2013
Kielkopf, J. F. 2000, Phys. Rev. E, 63, 016411
Kielkopf, J. F., & Allard, N. F. 1979, Phys. Rev. Lett., 43, 196
Kielkopf, J. F., & Allard, N. F. 1995, ApJ., 450, L75
Kielkopf, J. F., & Allard, N. F. 1998, Phys. Rev. A, 58, 4416
Kielkopf, J. F., & Allard, N. F. 2000, Connecticut meeting of the APS, Division of Atomic, Molecular, and Optical Physics, June 14-17
Kowalski, P. M. 2006, ApJ, 651, 1120
Kowalski, P. M., & Saumon, D. 2006, ApJ, 651, L137
Roberts, J. R., & Voigt, P. A. 1971, J. Res. Nat. Bur. Stand., 75A, 291
Royer, A. 1971, Phys. Rev. A, 3, 2044
Royer, A. 1978, Acta Phys. Pol. A, 54, 805
Sando, K. M., Doyle R. O., & Dalgarno A. 1969, ApJ, 157, L143
Sando, K. M., & Wormhoudt, J. G. 1973, Phys. Rev. A, 7, 1889
Spielfiedel, A. 2003, J. Mol. Spectrosc., 217, 162
Spielfiedel, A., Palmieri, P., & Mitrushenkov, A. O. 2004, Molec. Phys., 102, 21, 2249
Szudy, J., & Baylis, W. 1975, J. Quant. Spectrosc. Radiat. Transfer, 15, 641
Theodorakopoulos, G., Petsalakis, I. D., Nicolaides, C. A., & Buenker, R. J. 1987, J. Phys. B, 20, 2339
Wolff, B., Koester, D., & Liebert, J. 2002, A&A, 385, 995